KIM-1/TIM-1 is a Receptor for SARS-CoV-2 in Lung and Kidney

Takaharu Ichimura[1]*, Yutaro Mori[1]*, Philipp Aschauer[3], Krishna M. Padmanabha Das[3], Robert F. Padera Jr.[4], Astrid Weins[4], Mahmoud L. Nasr[1,2] and Joseph V. Bonventre[1,2,+]

*These authors contributed equally to this work.

[1]Division of Renal Medicine, Department of Medicine, Brigham and Women's Hospital, Harvard Medical School, Boston, MA 02115, USA

[2]Division of Engineering in Medicine, Department of Medicine, Brigham and Women's Hospital, Harvard Medical School, Boston, MA 02115, USA

[3]Department of Biological Chemistry and Molecular Pharmacology, Harvard Medical School, Boston, MA 02115, USA

[4]Department of Pathology, Brigham and Women's Hospital, Harvard Medical School, Boston, MA 02115, USA

[+] Corresponding author: Joseph V. Bonventre, MD, PhD

Samuel A. Levine Distinguished Professor of Medicine, Harvard Medical School

Constantine L. Hampers, MD Distinguished Chair in Renal Medicine

Chief, Division of Renal Medicine

Chief, Division of Engineering in Medicine

Department of Medicine, Brigham and Women's Hospital

4 Blackfan Circle Room 576, Boston, MA 02115

Phone : (617) 525-5966, Fax : (617) 525-5965

Email : joseph_bonventre@hms.harvard.edu

Summary

SARS-CoV-2 precipitates respiratory distress by infection of airway epithelial cells and is often accompanied by acute kidney injury. We report that Kidney Injury Molecule-1/T cell immunoglobulin mucin domain 1 (KIM-1/TIM-1) is expressed in lung and kidney epithelial cells in COVID-19 patients and is a receptor for SARS-CoV-2. Human and mouse lung and kidney epithelial cells express KIM-1 and endocytose nanoparticles displaying the SARS-CoV-2 spike protein (virosomes). Uptake was inhibited both by anti-KIM-1 antibodies and by TW-37, our newly discovered inhibitor of KIM-1-mediated endocytosis. Enhanced KIM-1 expression by human kidney tubuloids increased uptake of virosomes. KIM-1 positive cells express less angiotensin-converting enzyme 2 (ACE2), the well-known receptor for SARS-CoV-2. Using microscale thermophoresis, the EC50 for KIM-1-SARS-CoV-2 spike protein, and receptor binding domain (RBD) interactions, were 19 and 10 nM respectively. Thus KIM-1 is an alternative receptor to ACE2 for SARS-CoV-2. KIM-1 targeted therapeutics may prevent and/or treat COVID-19.

(147 words)

Keywords

Tubuloids, virosomes, spike protein, acute kidney injury, cytokine storm, IL-1β

Introduction

Coronavirus disease 2019 (COVID-19) caused by SARS-CoV-2 (2020b) was first reported at Wuhan in China in 2019 (Hui et al., 2020). The disease has reached pandemic proportions (2020c)(2020a). SARS-CoV-2-related respiratory failure and acute kidney injury (AKI) are major complications of infection (Chen et al., 2020a; Guan et al., 2020; Li et al., 2020) and are associated with high morbidity and mortality (Chen et al., 2020b; Cheng et al., 2020). **K**idney **I**njury **M**olecule**-1** (KIM-1) was identified by our group as the most upregulated protein in the kidney proximal tubule after a wide variety of injurious influences including ischemia, nephrotoxicants, sepsis and immune related injury and its cleaved ectodomain is often used as a serum and urine marker for kidney injury (Brooks et al., 2015; Ichimura et al., 1998; Ichimura et al., 2004; Sabbisetti et al., 2014; Takasu et al., 2013; Vaidya et al., 2010). KIM-1, also identified as Hepatitis A Virus Cellular Receptor 1 (HAVCR1) in hepatocytes (Kaplan et al., 1996), and T-cell immunoglobulin and mucin domain 1 (TIM-1), has been reported to be a receptor for Ebola virus (Kondratowicz et al., 2011), and Dengue virus (Meertens et al., 2012). KIM-1 also facilitates cellular uptake of West Nile virus (Jemielity et al., 2013). KIM-1 specifically mediates internalization and transduction of Marburg virus glycoprotein (GP) and full-length Ebola virus GP pseudovirions into human mucosal epithelia from the trachea (Kondratowicz et al., 2011). KIM-1-mediated infection was efficiently inhibited by anti-human KIM-1 IgV domain specific monoclonal antibody ARD5 (Bailly et al., 2002). In the kidney, KIM-1 acts as a receptor for phosphatidylserine exposed on the surface of apoptotic cells and for oxidized lipids (Ichimura et al., 2008). Once ligands bind to KIM-1, they are internalized by phagocytosis or endocytosis. Recently we have identified TW-37 as an inhibitor of KIM-1 mediated oxidized lipid and fatty acid (bound to albumin) uptake (Mori et al., 2020).

The SARS-CoV-2 envelope has a spike (S) glycoprotein, consisting of S1 and S2 subunits (Du et al., 2009). After infection the trimeric S protein is cleaved into the two subunits and S1, which contains the receptor binding domain, binds to angiotensin-converting enzyme 2 (ACE2) and is internalized by lung epithelium. In addition to ACE2, carcinoembryonic antigen-related cell adhesion molecule (CEACAM) is known to be a receptor for SARS-CoV (Krueger et al., 2001). KIM-1 has a N-terminus conserved IgV domain with has high homology with CEACAM's IgV domain where the S1 subunit binds (Lewicki and

Gallagher, 2002). T-cell immunoglobulin and mucin domain 3 (TIM-3), another KIM/TIM-family member protein, forms a heterodimer with CEACAM (Huang et al., 2015). Although KIM-1 is expressed at very high levels in the kidney, it has also been reported to be expressed in human primary airway epithelial cells in pulmonary disease, human non-small-cell lung cancer and human lung adenocarcinoma A549 cells (Thomas et al., 2016; Zheng et al., 2019). KIM-1 is also expressed in Vero E6 monkey kidney cells which have been used for *in vitro* expansion and maintenance of Coronavirus including SARS-CoV-2 as well as other viruses (Harcourt et al., 2020).

Here, we show that KIM-1 acts as a receptor for SARS-CoV-2 both in lung and kidney epithelia. KIM-1 expression in alveolar epithelium co-localizes in cells with SARS-CoV-2 nucleocapsid protein in post-mortem lung samples from COVID-19 patients. KIM-1 can bind to and mediate the internalization of liposomal nanoparticles displaying the SARS-CoV-2 spike protein ectodomain on their surface (virosomes) *in vitro*. The internalization of virosomes is inhibited both by anti-KIM-1 antibodies and TW-37. The EC50 for binding between the purified KIM-1 ectodomain and purified SARS-CoV-2 spike protein, and between the KIM-1 ectodomain and the RBD were 19 nM and 10 nM respectively. Thus KIM-1 may play an important role in viral infection and can be a potential therapeutic target to mitigate SARS-CoV-2's effects in both lung and kidney.

RESULTS

KIM-1 is expressed in COVID-19 patient autopsy lung samples.

KIM-1 was expressed in post-mortem lung of 10 of 11 patients who died and had SARS-CoV-2 infection. KIM-1 was present in pan-cytokeratin-positive alveolar epithelial cells which, in most cases, were dislodged and formed debris-like clusters. In two patients (Patient 1 and 2), positive staining for SARS-CoV-2 nucleocapsid protein was present in KIM-1-positive, pan-cytokeratin-positive and surfactant protein C-positive, alveolar epithelial cells (**Fig. 1A**). KIM-1 was detected using two different antibodies (AF1750 polyclonal and AKG7 monoclonal (Bailly et al., 2002)). ACE2, a well-known receptor for SARS-CoV-2, was expressed and, in patient 1, is seen co-localized with KIM-1 and pan-cytokeratin (**Fig. 1A**).

KIM-1 is expressed in COVID-19 patient biopsy and autopsy kidney proximal tubules.

Since AKI is a frequent manifestation of COVID-19, we evaluated KIM-1 expression in COVID-19 patient kidney biopsies from 3 live patients with AKI who survived their hospitalization and 30 post-mortem kidney samples from patients with documented SARS-CoV-2 infection during their terminal hospitalization. KIM-1 expression was seen in all 3 biopsy cases with approximately 10% of proximal tubules staining positive in both the cortex and outer medulla (**Fig. 1B and 1C**). Estimated GFR and brief description of the predominant renal pathology at the time of biopsy are presented in **Fig. 1C**. KIM-1 positive tubules were dilated with some tubules containing cellular debris. ACE2 is widely expressed on the apical side of proximal tubules in the same regions as KIM-1. KIM-1 positive tubules show reduced or no ACE2 staining, suggesting that ACE2 might be down-regulated as tubules dedifferentiate and express more KIM-1. We detected KIM-1 in 14 of 30 autopsy cases (**Fig. 1D**). In some patients, KIM-1 is expressed in relatively well-preserved tubules; however, in the majority of kidneys with KIM-1 expression the protein was localized in exfoliated tubular cells due to postmortem artifacts. In some cases, ACE2 was also detected in those exfoliated cells. Thus, in COVID-19 patients' kidneys, KIM-1 was frequently expressed, and significant tubular injury and KIM-1 expression were associated with less ACE2 expression in the proximal tubules. We compared this reciprocal response between KIM-1 and ACE2 to a well-established mouse model of AKI. When KIM-1 and ACE2 were stained in post ischemia-reperfusion injury (IRI) in mouse kidneys, ACE2

was down-regulated when KIM-1 is increased in flattened epithelial cells of the proximal tubules (**Fig. 1E**). In one of autopsy kidneys from a male in his fifties with an eGFR of 16 ml/min/1.73m^2, SARS-CoV-2 nucleocapsid protein was observed in focal areas of proximal tubules and intraluminal casts of cellular debris (**Fig. 1F and 1G**).

The role of KIM-1 in promotion of SARS-CoV-2 entry in lung alveolar epithelial cells.

SARS-CoV-2 virosomes were constructed of phospholipid liposomes conjugated to His-tagged spike ectodomain on their surfaces (**Fig. 2A**) and uptake of these fluorescently (DiI) labelled biomimetic viruses (virosomes, **Fig 2A**) was assessed *in vitro*. A549 cells, adenocarcinoma human alveolar basal epithelial cells, express KIM-1 and endocytosed SARS-CoV-2 virosomes while there was very little uptake of unconjugated empty liposomes (**Fig. 2B**) as assessed by confocal microscopy. Cellular uptake of virosomes was efficiently inhibited by treatment with anti-KIM-1 IgG or with TW-37, our newly discovered inhibitor for KIM-1-mediated endocytosis (Mori et al., 2020) (**Fig. 2C**). ACE2 was also expressed in A549 cells and was not altered in expression by anti-KIM-1 antibody (**Fig. 2D**). Virosomes were taken up by 92.3% ± 1.1% of A549 cells and anti-KIM-1 antibodies and TW-37 decreased the uptake to 44.9% ± 17.0% and 3.5% ± 0.2% respectively as quantitated by flow cytometry (**Fig. 2E**). We also analyzed uptake of virosomes by mouse primary lung epithelial cells. Cells were isolated from both wild-type mice and mice carrying a mutation in the KIM-1 mucin domain (KIM-1$^{\Delta mucin}$ mice) (Xiao et al., 2012). KIM-1$^{\Delta mucin}$ serves as a functional knockout with reduced epithelial cell uptake of known KIM-1 ligands (Brooks et al., 2015; Yang et al., 2015). Wild-type mouse primary lung epithelial cells took virosomes up efficiently, similar to A549 cells. Treatment with anti-KIM-1 antibody or TW-37 dramatically decreased the uptake of virosomes and KIM-1$^{\Delta mucin}$ cells showed significantly less uptake than wild-type cells (**Fig. 2F and 2G**).

The role of KIM-1 in promotion of SARS-CoV-2 entry into kidney cells.

Stably transfected LLC-PK1 pig kidney cell lines expressing human KIM-1 (hKIM-1-LLC-PK1) and controls without KIM-1 expression (pcDNA3-LLC-PK1) were incubated with fluorescence labeled SARS-CoV-2 spike protein conjugated virosomes. (**Fig. 3A**). The hKIM-1-LLC-PK1 cells endocytosed SARS-CoV-2

virosomes in a KIM-1 dependent manner, whereas there was no uptake of unconjugated empty liposomes (**Fig. 3A**) as assessed by confocal microscopy. Both hKIM-1-LLC-PK1 and pcDNA3-LLC-PK1 cells stained positively for ACE2; however, the ACE2 was not membrane associated. pcDNA3-LLC-PK1 control cells appeared to have more intense and defuse ACE2 staining, even though the cells did not demonstrate significant uptake of the virosomes when compared to the hKIM-1-LLC-PK1 cells (**Fig. 3B**). ACE2 protein expression was confirmed by western blot analysis of the cell lysates from both cell lines whereas KIM-1 was expressed only in the hKIM-1-LLC-PK1 cells (**Fig. 3C**). When ACE2 and KIM-1 were co-stained and analyzed in high magnification confocal microscope images ACE2 is found mainly in cytoplasm with small amounts on the cell surface, while KIM-1 expression is primarily on the cell surface (arrows) (**Fig. 3D**). TW-37 (10 μM) pretreatment for 30 min markedly reduced uptake of SARS-CoV-2 virosomes into hKIM-1-LLC-PK1 cells (**Fig. 3E**).

Three dimensional human renal epithelial tubuloids take up virosomes.

We have developed a method to make epithelial KIM-1 expressing “tubuloids” from kidney tissue derived from human subjects (Mori et al., 2020). Human primary epithelial cell cultures were established from the non-tumor kidney tissue removed from patients with renal cell carcinoma. Those primary cells were cultured in suspension with growth factors and Matrigel in non-adherent dishes (see Methods). KIM-1 expressing cells of human tubuloids took up DiI-labeled virosomes (**Fig 3F**). With uptake of spike conjugated virosomes, the tubuloids maintained their tubule-like three dimensional structures as seen in phase contrast images (**Fig. 3G**). Since well-developed tubuloids with polar epithelium reduce expression of KIM-1, likely due to progressive differentiation of the tubular epithelium, we enhanced human KIM-1 expression by infecting tubuloids with an adenovirus expressing KIM-1 (Adenovirus-KIM-1) or the control vector expressing β-galactosidase (β-GAL) (Adenovirus-β-GAL). Both viral vectors contained a GFP expression cDNA for tracing of viral infection and transgene expression in the infected cells. After 48 hours of infection, we added DiI-labelled virosomes to the tubuloids (**Fig. 3H**). Adenovirus-KIM-1 infected GFP-positive tubuloid cells showed a high level of uptake of virosomes (**Fig 3H**, left) and robust expression of KIM-1 protein (**Fig. 3H**, right). The KIM-1 infected tubuloids showed polarized expression of KIM-1 similar

to proximal tubules *in vivo* and also expressed ACE2 (**Fig. 3I**). In comparison to the Adenovirus-KIM-1 infected cells, control Adenovirus-β-GAL infected tubuloids showed no KIM-1 staining and no uptake of virosomes or oxidized LDL (data not shown). Uptake of virosomes by the tubuloids overexpressing KIM-1 was dose dependent (**Fig. 3J**). Quantification of ACE2 expression by flow cytometry on tubuloids infected by Adenovirus-KIM-1 or control Adenovirus-β-GAL, after digestion into single cells, revealed a mean 29.8% decrease on single cell ACE2 expression secondary to Adenovirus-KIM-1 infection (**Fig. 3K**). To test potential involvement of KIM-1 mediated viral uptake in the pro-inflammatory phenotype often seen with SARS-CoV-2 infection we treated tubuloids with the S1 subunit of the Spike protein and found KIM-1 dependent upregulation of intracellular interleukin-1β (IL-1β) (**Fig. 3L**).

KIM-1 binds SARS-COV2 Spike protein and receptor binding domain (RBD) *in vitro*.

KIM-1 binding to SARS-Cov2 spike protein ectodomain and GST-RBD was tested using Micro Scale Thermophoresis. The EC50 for interaction between KIM-1 ectodomain and the Spike ectodomain was 19 nM with a CI (95%) of 9 to 39 nM (**Fig. 4A and 4C**). Interaction of the KIM-1 ectodomain with GST-RBD showed an EC50 of 10 nM with a confidence interval (CI) (95%) from 6 to 16 nM (**Fig. 4B and 4C**).

DISCUSSION

We have found that KIM-1 serves as a receptor for SARS-CoV-2 virosomes in alveolar and kidney proximal tubule epithelial cells and uptake is inhibited by anti-KIM-1 antibodies or TW-37, an inhibitor for KIM-1-mediated endocytosis (Mori et al., 2020). Inhibition of this KIM-1 mediated uptake may be therapeutically useful in SARS-CoV-2 infection. The fact that KIM-1 binds to the spike protein of SARS-CoV-2 and virosomes stimulated IL-1β, an inflammatory mediator, in a KIM-1 dependent fashion suggests that KIM-1 may be involved in the pro-inflammatory state that can be so profound and has been associated with a “cytokine storm” (Moore and June, 2020). KIM-1 protein is detectable in partially autolyzed autopsy samples due to the protein’s stability (Yin et al., 2018). KIM-1 expressing proximal tubules have reduced expression of ACE2, the well-known receptor for SARS-CoV-2 (Hoffmann et al., 2020), suggesting that KIM-1 may alter ACE2-mediated viral entry into cells.

While the role of SARS-CoV-2 viral infection of kidney cells remains controversial, the implications of our findings extend beyond the kidney tubule cells since the ectodomain of KIM-1 enters the blood and can interact with the virus there. KIM-1 is upregulated by many insults to the kidney which result in AKI. We have shown that acute upregulation of KIM-1 with injury is protective likely due to an anti-inflammatory and anti-obstructive response associated with phagocytosis of apoptotic debris in the tubule (Yang et al., 2015). Our findings that KIM-1 is a receptor for SARS-CoV-2 indicate that KIM-1 could interact with exfoliated and virus infected cells in the lung and kidney. Furthermore, the KIM-1 ectodomain may bind to the virus in the pulmonary alveoli and kidney tubular lumen and could also act as a decoy receptor.

KIM-1 facilitated endocytosis of SARS-CoV-2 virosomes is both KIM-1 and spike protein dependent. Jemielity et al. demonstrated that the phosphatidylserine binding characteristics of human KIM-1/TIM-1 mediate its activity as a SARS-CoV-1 pseudovirus receptor (Jemielity et al., 2013). It is important to recognize, however, that the virosomes we used do not contain phosphatidylserine, so the interaction of KIM-1 with this phospholipid cannot explain the KIM-1 mediated facilitation of uptake. The high affinity interaction between the receptor binding domain of the S1 subunit with KIM-1 confirms that the KIM-1 mediated binding interaction is with the spike protein of SARS-CoV-2.

Our recently discovered KIM-1 small molecule inhibitor, TW-37, blocked KIM-1-mediated endocytosis

of SARS-CoV-2 virosomes in renal epithelial cells. TW-37 was originally discovered as a bcl-2 inhibitor in cancer drug screening, and has been found safe to use in animals (Ahn et al., 2019; Lei et al., 2017) . Our finding that TW-37 blocked entry of the SARS-CoV-2 virosomes suggests prevention of viral internalization as an approach to anti-SARS-CoV-2 viral treatment. This would be reminiscent of the use of Enfuvirtide, Maraviroc and Ibalizumab for HIV where administration of agents that will bind to the virus in the circulation will compete for tissue binding (Henrich and Kuritzkes, 2013).

Using our newly established three-dimensional renal epithelial tubuloid system we demonstrated uptake of the virosomes and enhancement of IL-1β production after tubuloid exposure to the SARS-CoV-2 spike protein. We have developed tubuloids as a way to make more homogeneous differentiated 3D epithelial-like structures of human kidney epithelial cells which maintain polarity and epithelial tight junctions. Tubuloids are created from human kidney cells in less than 2 weeks and overcome many of the shortcomings of cells that become dedifferentiated when placed in 2D culture. Tubuloids are readily infected for transgene expression while still maintaining functional integrity and allowing for demonstration of inflammatory responses. Infection with an adenovirus expressing KIM-1 enhanced membrane expression of KIM-1 and uptake of SARS-CoV-2 spike protein conjugated virosomes.

At the present time there is controversy with respect to the presence of SARS-CoV-2 nuclear capsid protein immunoreactivity in kidney tissue of subjects with documented infection with some investigators reporting its presence (Braun et al., 2020; Puelles et al., 2020) and others not finding evidence for virus in autopsy specimens (Santoriello et al., 2020; Sharma et al., 2020). SARS-CoV-2 RNA has been reported in 38 of 63 post-mortem kidneys of patients who had SARS-CoV-2 respiratory infection (Braun et al., 2020). We found clear evidence for viral infection in one patient but the infection was quite focal and could easily have been missed if the specimen was a biopsy during to sampling bias. It is possible there is early infection of the kidney but then the virus is cleared by the time the kidney specimen is obtained later in the course of illness in the patient who develops AKI or succumbs to the COVID-19 disease. This viral clearance has been reported to occur in the lung also (Schaefer et al., 2020). It is also possible that KIM-1-bound virus may shunt the virus to degradation pathways to destroy them, as occurs with HIV in macrophages (Gobeil et al., 2012). This is compatible with KIM-1 uptake of injurious material by

phagocytosis followed by degradation in a special autophagic pathway (Brooks et al., 2015). While KIM-1/TIM-1 mediated SARS-CoV-1 entry to the human cells has been reported to be facilitated by KIM-1, KIM-1 does not enhance infectivity (Jemielity et al., 2013). Our finding that the uptake of the spike protein promotes pro-inflammatory signaling, suggests, however, that even if the binding of the virus by KIM-1 does not promote infectivity it may be detrimental contributing the cytokine storm and worsening of the lung and kidney disease.

In conclusion, KIM-1 is a receptor for SARS-CoV-2 with a high affinity interaction with the receptor binding domain of the virus S1 subunit of the spike protein. KIM-1 dependent uptake by lung and kidney cells can be inhibited by anti-KIM-1 antibodies and TW-37. This may have important implications for viral entry, triggering of the cytokine storm, and/or inactivation of the virus through viral degradation or decoy function in the kidney and respiratory mucosa. Targeted treatment directed at the KIM-1-SARS-CoV-2 interaction may be both therapeutic and prophylactic for this devastating disease that occurs secondary to infection.

Acknowledgements

This work was supported by grants from the National Institute of Health/NCATS/NIDDK UH3TR002155 (J.V.B.); NIDDK 2R01DK072381 (J.V.B.), R37DK039773 (J.V.B.) and Postdoctoral Fellowship from Uehara Memorial Foundation (to Y.M.), and Overseas Research Fellowships from Japan Society for the Promotion of Science (to Y.M.). The authors would like to thank Zi-Fu Wang for help with binding experiments and thank Bing Chen and Youngfei Cai for providing purified spike ectodomain.

Author contributions

T.I., Y.M., P.A., K.M.P.D., R.F.P., A.W. and M.L.N. performed experiments, collected and analyzed data, and wrote the manuscript. R.F.P. and A.W. obtained human lung and kidney samples and helped to interpret the pathology. J.V.B. developed experimental strategy, supervised the project, and edited the manuscript. All authors discussed the results and implications and commented on the manuscript.

Competing Interests

J.V.B. and T.I. are co-inventors on KIM-1 patents assigned to Partners Healthcare. J.V.B. is a consultant to Cadent, Praxis and Seattle Genetics, Aldeyra, Angion and owns equity in Goldfinch, Innoviva, MediBeacon, DxNow, Verinano, Sensor Kinesis and Sentien.

Additional Information

Correspondence and requests for materials should be addressed to J.V.B..

Figure Legends

Figure 1. KIM-1 is expressed in COVID-19 patient alveolar and kidney epithelia.

(**A**) Representative immunostaining of KIM-1, SARS-CoV-2 nucleocapsid protein and pan-cytokeratin (top two rows), immunostaining of KIM-1 and SARS-CoV-2 nucleocapsid protein (3rd row), and immunostaining of ACE2, KIM-1, pan-cytokeratin and surfactant protein (bottom 2 panels) in kidney biopsy samples from COVID-19 patients. DAPI staining marks the nuclei in this and other panels. Scale bars, 20 μm.

(**B**) Immunostaining of KIM-1 and ACE2 in a post-mortem lung sample from COVID-10 patients. Scale bar, 20 μm.

(**C**) Patient information for three COVID1-19-associated AKI kidney biopsy samples. The patients' ages were at a range of 45-60 years old.

(**D**) Immunostaining of KIM-1 and ACE2 in representative post-mortem kidney biopsy samples from four COVID-19- patients. Scale bars, 20 μm.

(**E**) Immunostaining of KIM-1 and ACE2 post ischemia-reperfusion injury (IRI) in mouse kidneys. Scale bars, 20 μm.

(**F**) Immunohistochemistry staining of SARS-CoV-2 nucleocapsid protein in a COVID-19-associated AKI patient. Scale bars, 50 μm (left panel), 20 μm (right panel).

(**G**) Immunostaining of SARS-CoV-2 nucleocapsid protein in a COVID-19 post-mortem kidney section from the patient where immunohistochemisty is shown in **Fig 1F**. Scale bar, 20 μm.

Figure 2. SARS-CoV-2 virosomes containing the spike protein with both S1 and S2 subunits are internalized by lung epithelial cells and A549 adenocarcinoma human alveolar basal epithelial cells in a KIM-1-dependent manner.

(**A**) Negative-stain electron micrograph of SARS-CoV-2 virosomes displaying the spike ectodomain. The spike His-tag was bind to the nickel-nitrilotriacetic acid (Ni-NTA) lipids.

(**B**) A549 cell internalization of DiI-labeled virosomes as compared to control empty liposomes. Scale bars, 20 μm.

(**C**) Internalization of DiI-labeled virosomes by A549 cells in the presence of control mouse IgG, anti-KIM-

1 (3F4 and AKG7) or TW-37, a specific inhibitor for KIM-1, or control DMSO, immunostained with KIM-1
2 antibody (green). Scale bars, 20 μm.
3 (**D**) ACE2 immunostaining after uptake of DiI-labeled virosomes into A549 cells. Scale bars, 20 μm.
4 (**E**) Quantification of internalized DiI-labeled virosomes by A549 cells as measured by flow cytometry.
5 *p=0.0334, **p=0.0017.
6 (**F**) Internalization of DiI-labeled virosomes by mouse primary lung epithelial cells from wild-type mice or
7 KIM-1$^{\Delta mucin}$ mice after pretreatment with control IgG, anti-KIM-1 IgG (AF1817) or TW-37 or control DMSO.
8 Scale bars, 20 μm.
9 (**G**) Quantification of internalized DiI-labeled virosomes by mouse primary lung epithelial cells treated as
10 described in **Fig. 2F** and measured by ImageJ. Virosome-positive areas were normalized to the average
11 of wild-type cells treated with DMSO and control IgG. Ten fields were analyzed in two independent
12 experiments. *p<0.0001.
13
14 **Figure 3. SARS-CoV-2 virosomes are internalized by LLC-PK1 renal epithelial cells and human**
15 **kidney tubuloids in a KIM-1-dependent manner, and spike protein exposure results in IL-1β**
16 **production.**
17 (**A**) Internalization of DiI-labeled virosomes or control empty liposomes by LLC-PK1 cells stably expressing
18 KIM-1 or control pcDNA. Scale bars, 20 μm.
19 (**B**) Immunostaining of KIM-1 (AKG7) and ACE2 in LLC-PK1 cells stably expressing human KIM-1 or
20 control pcDNA. Scale bars, 20 μm.
21 (**C**) Western blotting of ACE2, KIM-1 (cytoplasmic domain, #195) and ERK1/2 on LLC-PK1 cells stably
22 expressing human KIM-1 or control pcDNA. Stars indicate the bands for each protein.
23 (**D**) Immunostaining of KIM-1 and ACE2 on LLC-PK1 cells stably expressing human KIM-1. Arrows indicate
24 that KIM-1 expression is located in cell surface. Scale bars, 10 μm.
25 (**E**) Internalization assay of DiI-labeled virosomes on LLC-PK1 cells stably expressing human KIM-1 with
26 pretreated with TW-37 or control DMSO. Scale bars, 20 μm.
27 (**F**) DiI-labeled virosome and control liposome internalization by human renal epithelial tubuloids,

immunostained with KIM-1 (green). Scale bars, 20 μm.

(**G**) Phase contrast images of human renal epithelial tubuloids treated with SARS-CoV-2 virosomes. There was no change in appearance as a result of virosome exposure. Scale bars, 20 μm.

(**H**) Internalization assay of DiI-labeled virosomes by human renal epithelial tubuloids infected by adenovirus expressing GFP-KIM-1 (left two panels) and immunostaining of KIM-1 and ACE2 on human renal epithelial tubuloids infected by adenovirus expressing GFP-KIM-1 or control GFP-β-GAL (right two panels). Scale bars, 20 μm.

(**I**) Immunostaining of KIM-1 and ACE2 in KIM-1 infected tubuloids. Scale bar, 20 μm.

(**J**) Internalization assay of DiI-labeled virosomes diluted to varying extents by human renal epithelial tubuloids infected with adenovirus expressing GFP-KIM-1. Scale bars, 20 μm.

(**K**) Quantification of ACE2 expression on tubuloids infected with adenovirus expressing GFP-KIM-1 or control GFP-β-GAL by flow cytometry. *$p<0.0001$.

(**L**) GFP expression and immunostaining of KIM-1 and IL-1β on human renal epithelial tubuloids infected with adenovirus expressing GFP-KIM-1 or control GFP-β-GAL after treatment with Spike S1 subunit for 24 hours. Scale bars, 20 μm.

Figure 4. KIM-1 binds SARS-CoV-2 Spike protein and RBD *in vitro*.

(**A**) Binding of SARS-CoV-2 Spike protein ectodomain with KIM-1 ectodomain. The calculated EC50 is 19nM with a CI (95%) of 9 to 39 nM.

(**B**) Binding of SARS-CoV-2 RBD GST fusion protein to KIM-1 ectodomain. The EC50 is 10 nM with a CI (95%) from 6 to 16 nM.

(**C**) SDS-PAGE of purified spike ectodomain, GST-RBD and KIM-1 used in the binding experiments.

STAR Methods

Human post-mortem samples and biopsy samples. Human postmortem lung and kidney samples from COVID-19 patients and human kidney biopsy samples from COVID-19-associated AKI patients were obtained from clinically indicated pathological autopsy and kidney biopsies in Brigham and Women's Hospital in Boston, US. The protocol was approved by the Institutional Review Board of the Ethics Committee of Partners Healthcare.

Immunofluorescence staining of paraffin sections. Human paraffin sections of postmortem samples or biopsy samples were deparaffinized with xylene, ethanol, 2% hydrogen peroxide in methanol to ablate peroxidase activity in a microwave oven. The sections were blocked with Avidin/Biotin Blocking Kit (Vector Laboratories, Burlingame, CA) and were incubated with primary antibodies for 1 hour at room temperature. After washing with PBS, sections were incubated with secondary antibodies for 30 minutes. Vectashield (Vector Laboratories, Burlingame, CA) containing DAPI (12.5 μg/ml) was applied and the slides were cover-slipped. All images were obtained by confocal microscopy (C1 Eclipse from Nikon).

Immunohistochemistry staining of KIM-1 in paraffin sections. Human paraffin sections of postmortem samples were deparaffinized with xylene, ethanol, 2% hydrogen peroxide in methanol to ablate peroxidase activity in a microwave oven. The sections were blocked with Avidin/Biotin Blocking Kit (Vector Laboratories, Burlingame, CA) and were incubated with primary antibody (AKG7) for 1 hour at room temperature. KIM-1 was detected using Vectastain Elite ABC kit (for mouse IgG) with DAB Substrate (Vector Laboratories, Burlingame, CA) kit for peroxidase staining. The sections were counterstained with hematoxylin and mounted with cover slips using Permount (Sigma-Aldrich, St. Louis, MO).

Mouse ischemia reperfusion injury (IRI). C57BL/6 mice were purchased from Charles River Laboratories. All mouse work was performed in accordance with the animal use protocol approved by the Institutional Animal Care and User Committee of the Harvard Medical School. Mice aged 8-12 weeks and weighing 20-22 g were subjected to IRI according to procedures as described previously (Brooks et

al., 2015; Park et al., 2003). Briefly, both kidneys were exposed by flank incisions, and the renal pedicles were clamped for 25 min at 37°C. Following surgery, 1 ml of warm saline (37°C) was injected intraperitoneally for volume supplement. Sham operations were performed by exposing both kidneys without clamping of renal pedicles. Kidney tissue was collected at 24 hours or 48 hours post IRI.

Cell culture experiments. Human primary renal epithelial cells were obtained from the uninvolved parts of kidneys removed for nephrectomy on the renal cell carcinoma or other kidney cancers in Brigham and Women's Hospital in Boston, US, by modifying a previously established protocol (Ichimura et al., 2008). The protocol was approved by the Institutional Review Board of the Ethics Committee of Partners Healthcare. Mouse primary lung epithelial cells were obtained and cultured by using the same protocol (Ichimura et al., 2008). Briefly, human renal cortex was diced, or mouse lung was taken out after sacrificed and was diced. They were digested with collagenase (0.5 mg/ml) in DMEM/F12 50:50 media for 40 minutes. The enzyme reaction was terminated with fetal bovine serum (FBS). Glomeruli and other remaining tissue clumps were separated from tubules by decanting the samples after gravity sedimentation (2 minutes). The remaining sample was washed 2 times in media and tubules were resuspended in tubular cell culture medium (DMEM/F12 with BSA, transferrin, insulin, selenium, hydrocortisone, and epidermal growth factor (EGF)). The epithelial cells were cultured for 7 to 14 days before being used for experiments.

LLC-PK1 cells stably expressing human KIM-1 were generated by transfecting LLC-PK1 cells with human KIM-1 full-length cDNA in the pcDNA vector (Ichimura et al., 2008). LLC-PK1 cells stably expressing empty pcDNA were used as controls.

GST-RBD expression and purification. The sequence coding for the RBD region of SARS-CoV-2 spike (331-524) was synthesized (Genscript, USA) along with TEV cleavage site at the N-terminal and Avi and His tags at the C-terminal. The gene was cloned into pGS21a vector at BamH1/NotI restriction sites. The resulting '6XHis-GST-TEV-RBD-Avi-6XHis' construct was transformed into BL21-Codon Plus (DE3) competent cells and the cultures were grown at 37 °C in LB medium containing Kanamycin to an OD_{600} of 0.6. Cells were cooled down to 16 °C and induced with 0.5 mM isopropyl β-D-1-thiogalactopyranoside.

Following overnight induction, cells were lysed in lysis buffer (20 mM Sodium phosphate buffer pH 7.4, 250 mM NaCl, 0.1% Titron X-100, 2.5 mM β mercaptoethanol) and purified using Ni affinity chromatography. The GST fusion protein was further purified by binding to Resource S ion-exchange column (GE Healthcare, USA) in the presence of (20 mM phosphate buffer pH 6.0, 50 mM NaCl, 1 mM DTT, 1mM EDTA), and eluting with a salt gradient, before loading onto a Superdex 200 column (GE Healthcare, USA) in a buffer containing 20 mM phosphate buffer pH 7.4, 137 mM NaCl, 1 mM DTT, 1 mM EDTA.

Virosomes assembly and purification. Purified SARS-CoV-2 spike ectodomain with deletion of the furin cleavage site, two proline mutations, a foldon trimerization domain and a C terminal His tag was used in the virosome assembly. Chloroform lipid stocks were mixed to accomplish the following ratio 15% 1,2-dioleoyl-sn-glycero-3-[(N-(5-amino-1-carboxypentyl) iminodiacetic acid) succinyl] (nickel, Ni, salt) (18:1DGS nickel-nitrilotriacetic acid (NTA) Ni)/51% 2-oleoyl-1-pamlitoyl-sn-glycero-3-phosphocholine (POPC)/34% 2-oleoyl-1-pamlitoyl-sn-glycero-3-glycerol (POPG). The mixture was dried under argon stream and stored in a desiccator overnight. The next day the mixture was resuspended in PBS buffer to achieve a final lipid concentration of 10 mM, the resulting milky solution was repeatedly pushed through a 0.1 μm filter membrane using an extruder until the solution was turned clear. The resulting liposome solution was calculated to have a concentration of approximately 100 nM. Liposomes were mixed with the His-tagged Spike ectodomain to achieve a ratio of 40:1 (spike-trimer: liposome) The mixture was incubated for 30 min on 4 °C to allow the spike His-tag to bind to the Ni-NTA lipids. Free spike protein was separated from spike loaded liposomes using a Superose 6 10/300 size exclusion chromatography column.

MST binding. KIM-1 (R&D, 1750-TM) was diluted with PBS to 200 nM. 100 μL of 200 nM. KIM-1 was mixed with 100 μl 100 nM RED-tris-NTA 2nd Generation dye (Nano Temper) dissolved in PBS, the mixture was incubated for 30 min on ice. The resulting labeled KIM-1 was further diluted to 10 nM. 1:1 serial dilutions were made for Spike-ecto domain in PBS with a starting concentration of 1 μM. 10 μl of each dilution for the Spike protein were mixed with 10 μl of 10 nM labeled KIM-1. The resulting mixtures were loaded in coated capillary (coated in house) and measured using a Monolith Pico (Nano Temper). The

samples were measured using the pico-red channel on medium MST power and excitation power 20%. For GST-RBD interaction with KIM-1, we followed the same procedure as above with the difference that GST-RBD was labeled was RED-tris-NTA and KIM-1 was used for the serial dilution. The excitation power used for GST-RBD was 60%. The highest concentration of the dilution series was 3.3 μM. Processing of the raw data was done in Microsoft Excel, data points between 5 s and 10 s were averaged. The results were normalized between 0 and 1 and exported to GraphPad where nonlinear fitting and calculation of the EC50 was done.

Internalization assay of virosomes and control empty liposomes. Cells were seeded onto 8-well chamber slide at a density of 1-1.5 x 10^5 cells/well (LLC-PK1 cells stably expressing human KIM-1 or empty pcDNA, A549 cells or mouse primary lung epithelial cells). After the cells become close to confluent, the cells were treated with 10 μM TW-37 or control DMSO for 30 minutes, or with 10 μM TW-37 or control DMSO in DMEM/F-12 media, and 0.025 mg/mL anti-KIM-1 mouse IgG (3F4) and 0.025 mg/mL anti KIM-1 mouse IgG (AKG7), or 0.05 mg/mL control mouse IgG in DMEM/F-12 media for 1 hour as pretreatment. Then virosomes or control empty liposomes were added at a ratio of 1:10 to media, and cells were incubated for 1.5 hours at 37 degree. After exposure to liposomes, the cells were washed with PBS and fixed with 4% paraformaldehyde (PFA)-PBS. Immunofluorescence staining of the cells was performed according to each experiment. For quantification of internalization from images taken by confocal microscopy, virosome-positive areas were measured by ImageJ and analyzed statistically.

For quantification of internalization by flowcytometry, A549 cells were seeded onto 12-well plates at a density of 4 x 10^5 cells/well. After the cells become mostly confluent, the cells were treated with 10 μM TW-37 or control DMSO in DMEM/F-12 media, and 0.025 mg/mL anti-KIM-1 mouse IgG (3F4) and 0.025 mg/mL anti KIM-1 mouse IgG (AKG7), or 0.05 mg/mL control mouse IgG in DMEM/F-12 media for 1 hour as pretreatment. Then virosomes or control empty liposomes were added at a ratio of 1:10 to media, and cells were incubated for 1.5 hours at 37 degree. After exposure to liposomes, the cells were washed with PBS and detached with 0.25% Trypsin/0.1% EDTA, fixed with 4% paraformaldehyde/5% FBS in PBS, and then immunostained with anti-KIM-1 and anti-ACE2 antibodies. Cells were analyzed by FACS Canto II (BD

Biosciences). Data were analyzed using FLOWJO (FLOWJO).

Immunofluorescence staining of cells. After fixation with 4% PFA-PBS, the cells were permeabilized with 0.1% Triton X-100-PBS and blocked with 3% BSA-PBS for 30 minutes. Primary antibodies were applied and the slides were incubated for 1 hour at room temperature or overnight at 4 degree. After washing with PBS, the slides were exposed to secondary antibodies and incubated for 30 minutes at room temperature. All images were obtained by confocal microscopy (C1 Eclipse from Nikon).

Antibodies. In immunofluorescence staining, primary antibodies against the following proteins were used: human KIM-1 (goat, 1:200, AF1750; R&D systems Inc, Minneapolis, MN); human KIM-1 (mouse, 1:1, AKG7 (Bailly et al., 2002), developed in collaboration with BIOGEN Inc. Cambridge, MA); mouse KIM-1 (goat, 1:200, AF1817; R&D systems Inc, Minneapolis, MN); SARS Coronavirus Nucleocapsid (rabbit, 1:200, PA1-41098; Invitrogen, Thermo Fisher Scientific, Waltham, MA); ACE2 (rabbit, 1:200, ab15348; Abcam, Cambridge, MA); Prosurfactant Protein C (rabbit, 1:200, ab90716; Abcam, Cambridge, MA); IL-1β (goat, 1:200, AF-201; R&D systems Inc, Minneapolis, MN). Secondary antibodies were either FITC-, Cy3- or Cy5- conjugated (Jackson ImmunoResearch Inc., West Grove, PA). In western blotting, primary antibodies against the following proteins were used: ACE2 (1:1000, as used in immunofluorescence staining); human KIM-1 cytoplasmic domain (rabbit, 1:1000, #195, developed in collaboration with BIOGEN Inc. Cambridge, MA (Zhang et al., 2007)); ERK1/2 (goat, 1:1000, Santa Cruz Biotechnology, Dallas, TX). As secondary antibodies, HRP-conjugated anti-rabbit IgG and anti-goat IgG (Dako, Denmark) were used. For inhibition of KIM-1 by antibodies, purified anti-human KIM-1 IgG (both mouse monoclonal AKG7 and 3F4, developed by our group) or anti-mouse KIM-1 IgG (AF1817) were used. Control mouse IgG was purchased from Jackson ImmunoResearch Inc. (West Grove, PA).

Western blotting. Cells and kidneys were lysed and protein was purified as previously described (Ichimura et al., 1998). Bands were visualized by chemiluminescence (Western Lightning, PerkinElmer, Waltham, MA).

Human renal tubuloids. The manuscript on the protocol to make human renal tubuloids is in preparation. Briefly, human primary renal epithelial cells were cultured on ultra-low attachment plates with 5% FBS-RPMI. After 2-3 days incubation, Matrigel was added and media was changed to 5% FBS-Advanced RPMI containing EGF, bFGF and HGF. Media was changed once or twice a week. The tubuloids are ready for use after 2 weeks. Adenoviruses for expression of human KIM-1 or control β-galactosidase (β-GAL) were produced and stored as described previously (Zhang et al., 2007). For detection of IL-1β induced by treatment with Spike S1 subunit protein, tubuloids infected by adenovirus for GFP and KIM-1 or for control GFP and β-GAL were treated with biotinylated 2019-nCoV S1 protein, His, Avitag (AcroBiosystems, DE) for 24 hours and immunostained.

Cell lines and reagents. LLC-PK1 cell lines and A549 cell lines were obtained from the ATCC. FBS, DMEM, and DMEM/F-12 were from Cellgro (Manassas, VA). TW-37 was purchased from Selleck Chemicals (Houston, TX). For labeling the virosomes and empty liposomes, CellTracker CM-DiI was purchased from Molecular Probes, Inc (Eugene, OR).

Statistical methods. Data are reported as mean ± standard error of the mean (SEM). Number of samples assayed in each experiment is indicated in the Figure Legends. Tukey-Kramer Multiple Comparisons Test was used for multiple comparisons. $p<0.05$ was considered to represent a statistically significant difference. Prism 8 (GraphPad Software, LLC) was used for all the statistical analysis.

Resource Availability

Lead Contact

Further information and requests for resources and reagents should be directed to and will be fulfilled by the Lead Contact, Joseph V. Bonventre (joseph_bonventre@hms.harvard.edu).

Material Availability

This study did not generate new unique reagents.

Data and Code Availability

All other data are available from the Lead Contact on reasonable request.

References

(2020a). Coronavirus COVID-19 Global Cases by the Center for Systems Science and Engineering (CSSE) at Johns Hopkins University (JHU). (Johns Hopkins Coronavirus Resource Center).

(2020b). Naming the coronavirus disease (COVID-19) and the virus that causes it. (World Health Organization).

(2020c). WHO Director-General's opening remarks at the media briefing on COVID-19 - 11 March 2020. (World Health Organization).

Ahn, C.H., Lee, W.W., Jung, Y.C., Shin, J.A., Hong, K.O., Choi, S., Swarup, N., Kim, J., Ahn, M.H., Jung, M., et al. (2019). Antitumor effect of TW-37, a BH3 mimetic in human oral cancer. Lab Anim Res *35*, 27.

Bailly, V., Zhang, Z., Meier, W., Cate, R., Sanicola, M., and Bonventre, J.V. (2002). Shedding of kidney injury molecule-1, a putative adhesion protein involved in renal regeneration. The Journal of biological chemistry *277*, 39739-39748.

Braun, F., Lütgehetmann, M., Pfefferle, S., Wong, M.N., Carsten, A., Lindenmeyer, M.T., Nörz, D., Heinrich, F., Meißner, K., Wichmann, D., et al. (2020). SARS-CoV-2 renal tropism associates with acute kidney injury. The Lancet.

Brooks, C.R., Yeung, M.Y., Brooks, Y.S., Chen, H., Ichimura, T., Henderson, J.M., and Bonventre, J.V. (2015). KIM-1-/TIM-1-mediated phagocytosis links ATG5-/ULK1-dependent clearance of apoptotic cells to antigen presentation. Embo j *34*, 2441-2464.

Chen, N., Zhou, M., Dong, X., Qu, J., Gong, F., Han, Y., Qiu, Y., Wang, J., Liu, Y., Wei, Y., et al. (2020a). Epidemiological and clinical characteristics of 99 cases of 2019 novel coronavirus pneumonia in Wuhan, China: a descriptive study. Lancet *395*, 507-513.

Chen, T., Wu, D., Chen, H., Yan, W., Yang, D., Chen, G., Ma, K., Xu, D., Yu, H., Wang, H., et al. (2020b). Clinical characteristics of 113 deceased patients with coronavirus disease 2019: retrospective study. BMJ *368*, m1091.

Cheng, Y., Luo, R., Wang, K., Zhang, M., Wang, Z., Dong, L., Li, J., Yao, Y., Ge, S., and Xu, G. (2020). Kidney impairment is associated with in-hospital death of COVID-19 patients. medRxiv, 2020.2002.2018.20023242.

Du, L., He, Y., Zhou, Y., Liu, S., Zheng, B.J., and Jiang, S. (2009). The spike protein of SARS-CoV--a target for vaccine and therapeutic development. Nat Rev Microbiol *7*, 226-236.

Gobeil, L.A., Lodge, R., and Tremblay, M.J. (2012). Differential HIV-1 endocytosis and susceptibility to virus infection in human macrophages correlate with cell activation status. J Virol *86*, 10399-10407.

Guan, W.J., Ni, Z.Y., Hu, Y., Liang, W.H., Ou, C.Q., He, J.X., Liu, L., Shan, H., Lei, C.L., Hui, D.S.C., et al. (2020). Clinical Characteristics of Coronavirus Disease 2019 in China. N Engl J Med *382*, 1708-1720.

Harcourt, J., Tamin, A., Lu, X., Kamili, S., Sakthivel, S.K., Murray, J., Queen, K., Tao, Y., Paden, C.R., Zhang, J., et al. (2020). Severe Acute Respiratory Syndrome Coronavirus 2 from Patient with 2019 Novel Coronavirus Disease, United States. Emerg Infect Dis *26*.

Henrich, T.J., and Kuritzkes, D.R. (2013). HIV-1 entry inhibitors: recent development and clinical use. Curr Opin Virol *3*, 51-57.

Hoffmann, M., Kleine-Weber, H., Schroeder, S., Kruger, N., Herrler, T., Erichsen, S., Schiergens, T.S., Herrler, G., Wu, N.H., Nitsche, A., et al. (2020). SARS-CoV-2 Cell Entry Depends on ACE2 and TMPRSS2 and Is Blocked by a Clinically Proven Protease Inhibitor. Cell *181*, 271-280 e278.

Huang, Y.H., Zhu, C., Kondo, Y., Anderson, A.C., Gandhi, A., Russell, A., Dougan, S.K., Petersen, B.S., Melum, E., Pertel, T., et al. (2015). CEACAM1 regulates TIM-3-mediated tolerance and exhaustion. Nature *517*, 386-390.

Hui, D.S., E, I.A., Madani, T.A., Ntoumi, F., Kock, R., Dar, O., Ippolito, G., McHugh, T.D., Memish, Z.A., Drosten, C., et al. (2020). The continuing 2019-nCoV epidemic threat of novel coronaviruses to global health - The latest 2019 novel coronavirus outbreak in Wuhan, China. Int J Infect Dis *91*, 264-266.

Ichimura, T., Asseldonk, E.J., Humphreys, B.D., Gunaratnam, L., Duffield, J.S., and Bonventre, J.V. (2008). Kidney injury molecule-1 is a phosphatidylserine receptor that confers a phagocytic phenotype on epithelial cells. J Clin Invest *118*, 1657-1668.

Ichimura, T., Bonventre, J.V., Bailly, V., Wei, H., Hession, C.A., Cate, R.L., and Sanicola, M. (1998). Kidney injury

molecule-1 (KIM-1), a putative epithelial cell adhesion molecule containing a novel immunoglobulin domain, is up-regulated in renal cells after injury. J Biol Chem *273*, 4135-4142.
Ichimura, T., Hung, C.C., Yang, S.A., Stevens, J.L., and Bonventre, J.V. (2004). Kidney injury molecule-1: a tissue and urinary biomarker for nephrotoxicant-induced renal injury. American journal of physiology. Renal physiology *286*, F552-563.
Jemielity, S., Wang, J.J., Chan, Y.K., Ahmed, A.A., Li, W., Monahan, S., Bu, X., Farzan, M., Freeman, G.J., Umetsu, D.T., et al. (2013). TIM-family proteins promote infection of multiple enveloped viruses through virion-associated phosphatidylserine. PLoS Pathog *9*, e1003232.
Kaplan, G., Totsuka, A., Thompson, P., Akatsuka, T., Moritsugu, Y., and Feinstone, S.M. (1996). Identification of a surface glycoprotein on African green monkey kidney cells as a receptor for hepatitis A virus. Embo j *15*, 4282-4296.
Kondratowicz, A.S., Lennemann, N.J., Sinn, P.L., Davey, R.A., Hunt, C.L., Moller-Tank, S., Meyerholz, D.K., Rennert, P., Mullins, R.F., Brindley, M., et al. (2011). T-cell immunoglobulin and mucin domain 1 (TIM-1) is a receptor for Zaire Ebolavirus and Lake Victoria Marburgvirus. Proc Natl Acad Sci U S A *108*, 8426-8431.
Krueger, D.K., Kelly, S.M., Lewicki, D.N., Ruffolo, R., and Gallagher, T.M. (2001). Variations in disparate regions of the murine coronavirus spike protein impact the initiation of membrane fusion. J Virol *75*, 2792-2802.
Lei, S., Ding, Y., Fu, Y., Wu, S., Xie, X., Wang, C., and Liang, H. (2017). The preclinical analysis of TW-37 as a potential anti-colorectal cancer cell agent. PLoS One *12*, e0184501.
Lewicki, D.N., and Gallagher, T.M. (2002). Quaternary structure of coronavirus spikes in complex with carcinoembryonic antigen-related cell adhesion molecule cellular receptors. The Journal of biological chemistry *277*, 19727-19734.
Li, Z., Wu, M., Guo, J., Yao, J., Liao, X., Song, S., Han, M., Li, J., Duan, G., Zhou, Y., et al. (2020). Caution on Kidney Dysfunctions of 2019-nCoV Patients. medRxiv, 2020.2002.2008.20021212.
Meertens, L., Carnec, X., Lecoin, M.P., Ramdasi, R., Guivel-Benhassine, F., Lew, E., Lemke, G., Schwartz, O., and Amara, A. (2012). The TIM and TAM families of phosphatidylserine receptors mediate dengue virus entry. Cell Host Microbe *12*, 544-557.
Moore, J.B., and June, C.H. (2020). Cytokine release syndrome in severe COVID-19. Science *368*, 473-474.
Mori, Y., Ajay, A.K., Chang, J.H., Mou, S., Zhao, H., Kishi, S., Li, J., Brooks, C.R., Xiao, S., Woo, H.M., et al. (2020). KIM-1 Mediated Tubular Fatty Acid Uptake Leads to Progressive Diabetic Kidney Disease. SSRN Electronic Journal.
Park, K.M., Byun, J.Y., Kramers, C., Kim, J.I., Huang, P.L., and Bonventre, J.V. (2003). Inducible nitric-oxide synthase is an important contributor to prolonged protective effects of ischemic preconditioning in the mouse kidney. The Journal of biological chemistry *278*, 27256-27266.
Puelles, V.G., Lutgehetmann, M., Lindenmeyer, M.T., Sperhake, J.P., Wong, M.N., Allweiss, L., Chilla, S., Heinemann, A., Wanner, N., Liu, S., et al. (2020). Multiorgan and Renal Tropism of SARS-CoV-2. N Engl J Med *383*, 590-592.
Sabbisetti, V.S., Waikar, S.S., Antoine, D.J., Smiles, A., Wang, C., Ravisankar, A., Ito, K., Sharma, S., Ramadesikan, S., Lee, M., et al. (2014). Blood kidney injury molecule-1 is a biomarker of acute and chronic kidney injury and predicts progression to ESRD in type I diabetes. J Am Soc Nephrol *25*, 2177-2186.
Santoriello, D., Khairallah, P., Bomback, A.S., Xu, K., Kudose, S., Batal, I., Barasch, J., Radhakrishnan, J., D'Agati, V., and Markowitz, G. (2020). Postmortem Kidney Pathology Findings in Patients with COVID-19. J Am Soc Nephrol.
Schaefer, I.M., Padera, R.F., Solomon, I.H., Kanjilal, S., Hammer, M.M., Hornick, J.L., and Sholl, L.M. (2020). In situ detection of SARS-CoV-2 in lungs and airways of patients with COVID-19. Mod Pathol.
Sharma, P., Uppal, N.N., Wanchoo, R., Shah, H.H., Yang, Y., Parikh, R., Khanin, Y., Madireddy, V., Larsen, C.P., Jhaveri, K.D., et al. (2020). COVID-19-Associated Kidney Injury: A Case Series of Kidney Biopsy Findings. J Am Soc Nephrol.
Takasu, O., Gaut, J.P., Watanabe, E., To, K., Fagley, R.E., Sato, B., Jarman, S., Efimov, I.R., Janks, D.L., Srivastava,

A., et al. (2013). Mechanisms of cardiac and renal dysfunction in patients dying of sepsis. Am J Respir Crit Care Med *187*, 509-517.
Thomas, L.J., Vitale, L., O'Neill, T., Dolnick, R.Y., Wallace, P.K., Minderman, H., Gergel, L.E., Forsberg, E.M., Boyer, J.M., Storey, J.R., et al. (2016). Development of a Novel Antibody-Drug Conjugate for the Potential Treatment of Ovarian, Lung, and Renal Cell Carcinoma Expressing TIM-1. Mol Cancer Ther *15*, 2946-2954.
Vaidya, V.S., Ozer, J.S., Dieterle, F., Collings, F.B., Ramirez, V., Troth, S., Muniappa, N., Thudium, D., Gerhold, D., Holder, D.J., et al. (2010). Kidney injury molecule-1 outperforms traditional biomarkers of kidney injury in preclinical biomarker qualification studies. Nat Biotechnol *28*, 478-485.
Xiao, S., Brooks, C.R., Zhu, C., Wu, C., Sweere, J.M., Petecka, S., Yeste, A., Quintana, F.J., Ichimura, T., Sobel, R.A., et al. (2012). Defect in regulatory B-cell function and development of systemic autoimmunity in T-cell Ig mucin 1 (Tim-1) mucin domain-mutant mice. Proc Natl Acad Sci U S A *109*, 12105-12110.
Yang, L., Brooks, C.R., Xiao, S., Sabbisetti, V., Yeung, M.Y., Hsiao, L.L., Ichimura, T., Kuchroo, V., and Bonventre, J.V. (2015). KIM-1-mediated phagocytosis reduces acute injury to the kidney. The Journal of clinical investigation *125*, 1620-1636.
Yin, W., Zhang, P.L., Macknis, J.K., Lin, F., and Bonventre, J.V. (2018). Kidney injury molecule-1 identifies antemortem injury in postmortem adult and fetal kidney. American journal of physiology. Renal physiology *315*, F1637-F1643.
Zhang, Z., Humphreys, B.D., and Bonventre, J.V. (2007). Shedding of the urinary biomarker kidney injury molecule-1 (KIM-1) is regulated by MAP kinases and juxtamembrane region. J Am Soc Nephrol *18*, 2704-2714.
Zheng, X., Xu, K., Chen, L., Zhou, Y., and Jiang, J. (2019). Prognostic value of TIM-1 expression in human non-small-cell lung cancer. J Transl Med *17*, 178.

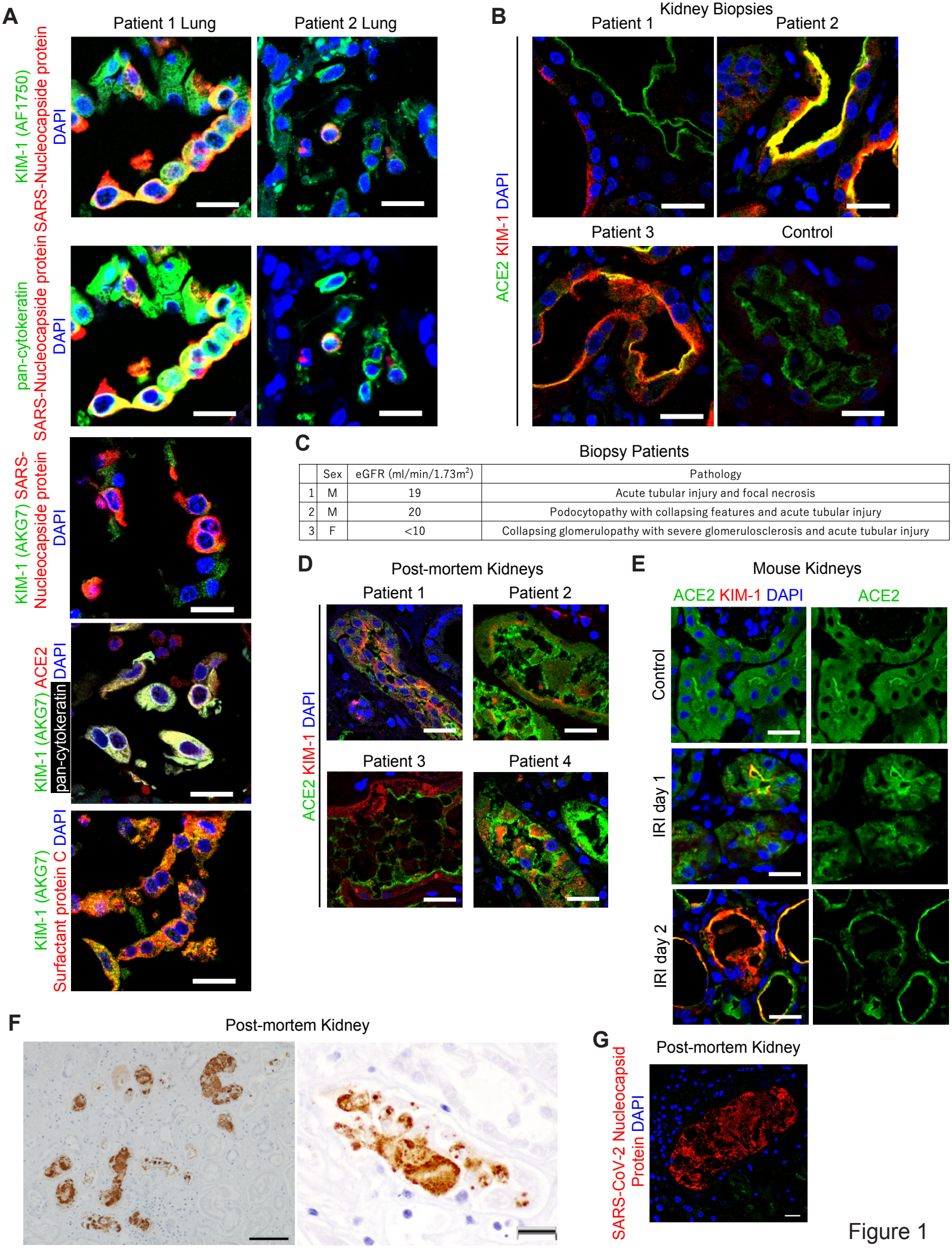

	Sex	eGFR (ml/min/1.73m^2)	Pathology
1	M	19	Acute tubular injury and focal necrosis
2	M	20	Podocytopathy with collapsing features and acute tubular injury
3	F	<10	Collapsing glomerulopathy with severe glomerulosclerosis and acute tubular injury

Figure 1

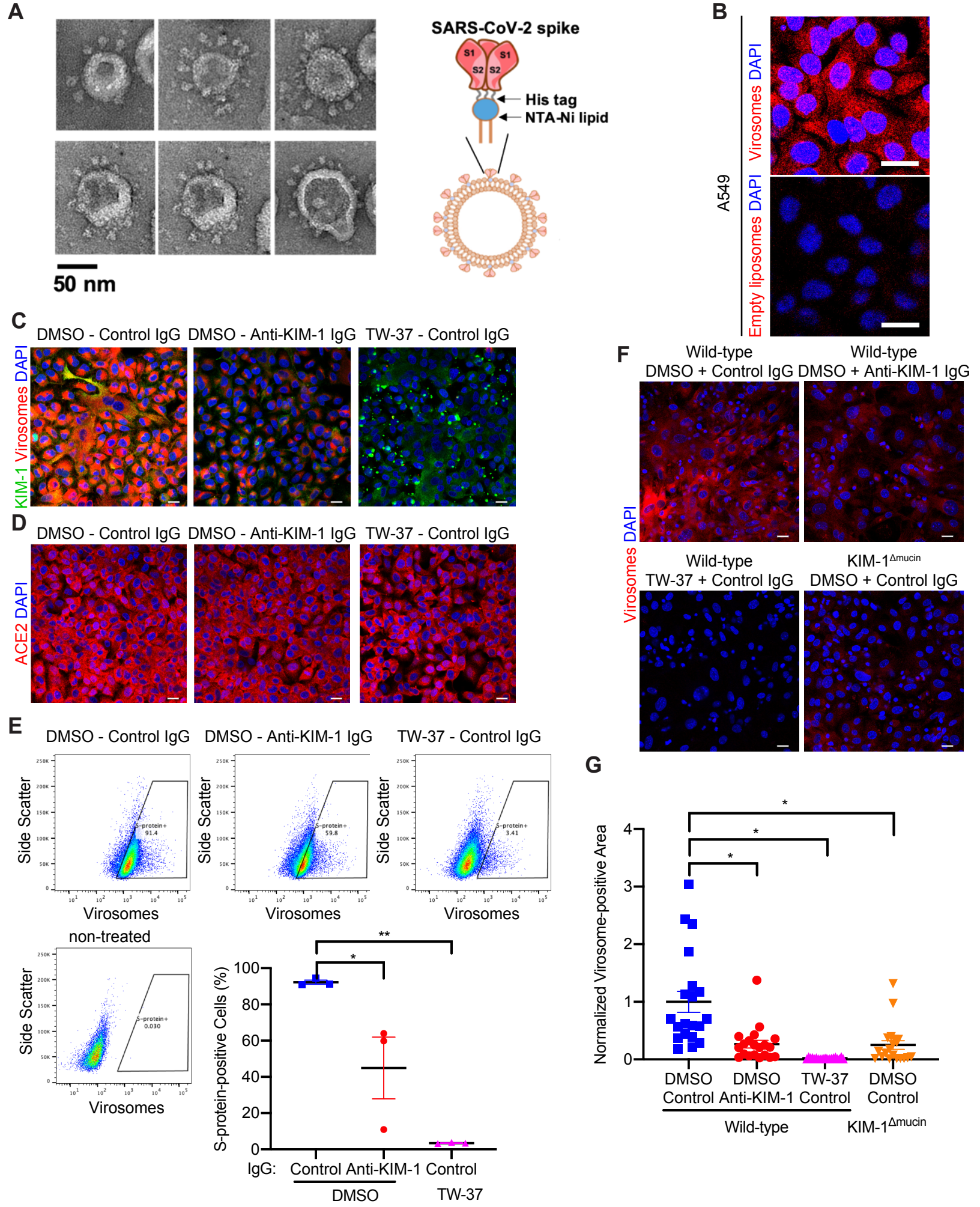
A
50 nm
SARS-CoV-2 spike
S1
S2
His tag
NTA-Ni lipid
B
A549
Virosomes DAPI
Empty liposomes DAPI
C
DMSO - Control IgG
DMSO - Anti-KIM-1 IgG
TW-37 - Control IgG
KIM-1 Virosomes DAPI
D
DMSO - Control IgG
DMSO - Anti-KIM-1 IgG
TW-37 - Control IgG
ACE2 DAPI
E
DMSO - Control IgG
DMSO - Anti-KIM-1 IgG
TW-37 - Control IgG
Side Scatter
Virosomes
S-protein+ 91.4
S-protein+ 59.8
S-protein+ 3.41
non-treated
S-protein+ 0.030
S-protein-positive Cells (%)
IgG: Control Anti-KIM-1 Control
DMSO
TW-37
F
Wild-type DMSO + Control IgG
Wild-type DMSO + Anti-KIM-1 IgG
Wild-type TW-37 + Control IgG
KIM-1Δmucin DMSO + Control IgG
Virosomes DAPI
G
Normalized Virosome-positive Area
DMSO Control
DMSO Anti-KIM-1
TW-37 Control
DMSO Control
Wild-type
KIM-1Δmucin

Figure 2

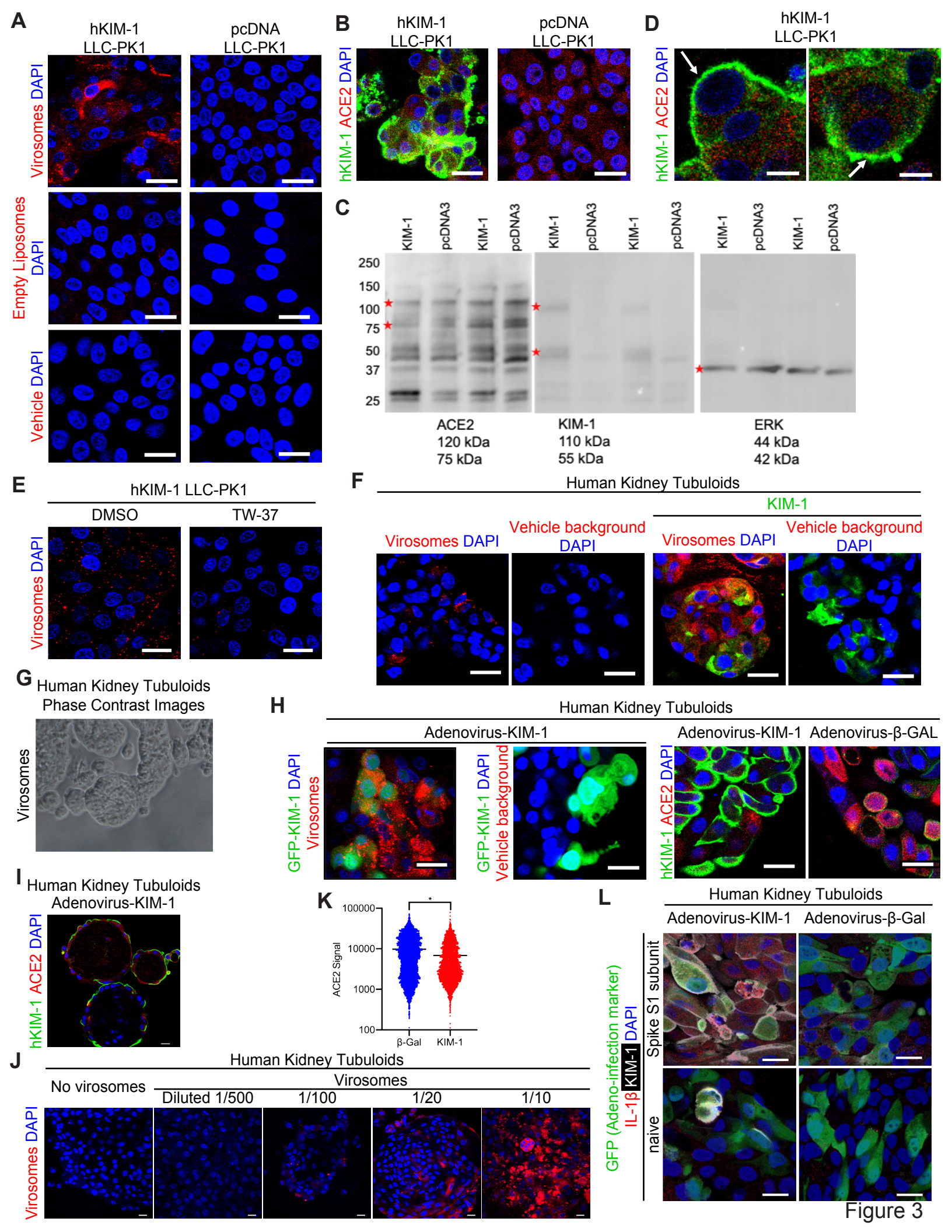
A
hKIM-1 LLC-PK1
pcDNA LLC-PK1
Virosomes DAPI
Empty Liposomes DAPI
Vehicle DAPI
B
hKIM-1 LLC-PK1
pcDNA LLC-PK1
hKIM-1 ACE2 DAPI
D
hKIM-1 LLC-PK1
hKIM-1 ACE2 DAPI
C
KIM-1
pcDNA3
250
150
100
75
50
37
25
ACE2
120 kDa
75 kDa
KIM-1
110 kDa
55 kDa
ERK
44 kDa
42 kDa
E
hKIM-1 LLC-PK1
DMSO
TW-37
Virosomes DAPI
F
Human Kidney Tubuloids
KIM-1
Virosomes DAPI
Vehicle background DAPI
G
Human Kidney Tubuloids
Phase Contrast Images
Virosomes
H
Human Kidney Tubuloids
Adenovirus-KIM-1
Adenovirus-β-GAL
GFP-KIM-1 DAPI
Virosomes
Vehicle background
hKIM-1 ACE2 DAPI
I
Human Kidney Tubuloids
Adenovirus-KIM-1
hKIM-1 ACE2 DAPI
K
100000
10000
1000
100
ACE2 Signal
β-Gal
KIM-1
L
Human Kidney Tubuloids
Adenovirus-KIM-1
Adenovirus-β-Gal
GFP (Adeno-infection marker)
IL-1β KIM-1 DAPI
Spike S1 subunit
naive
J
Human Kidney Tubuloids
No virosomes
Virosomes
Diluted 1/500
1/100
1/20
1/10
Virosomes DAPI

Figure 3

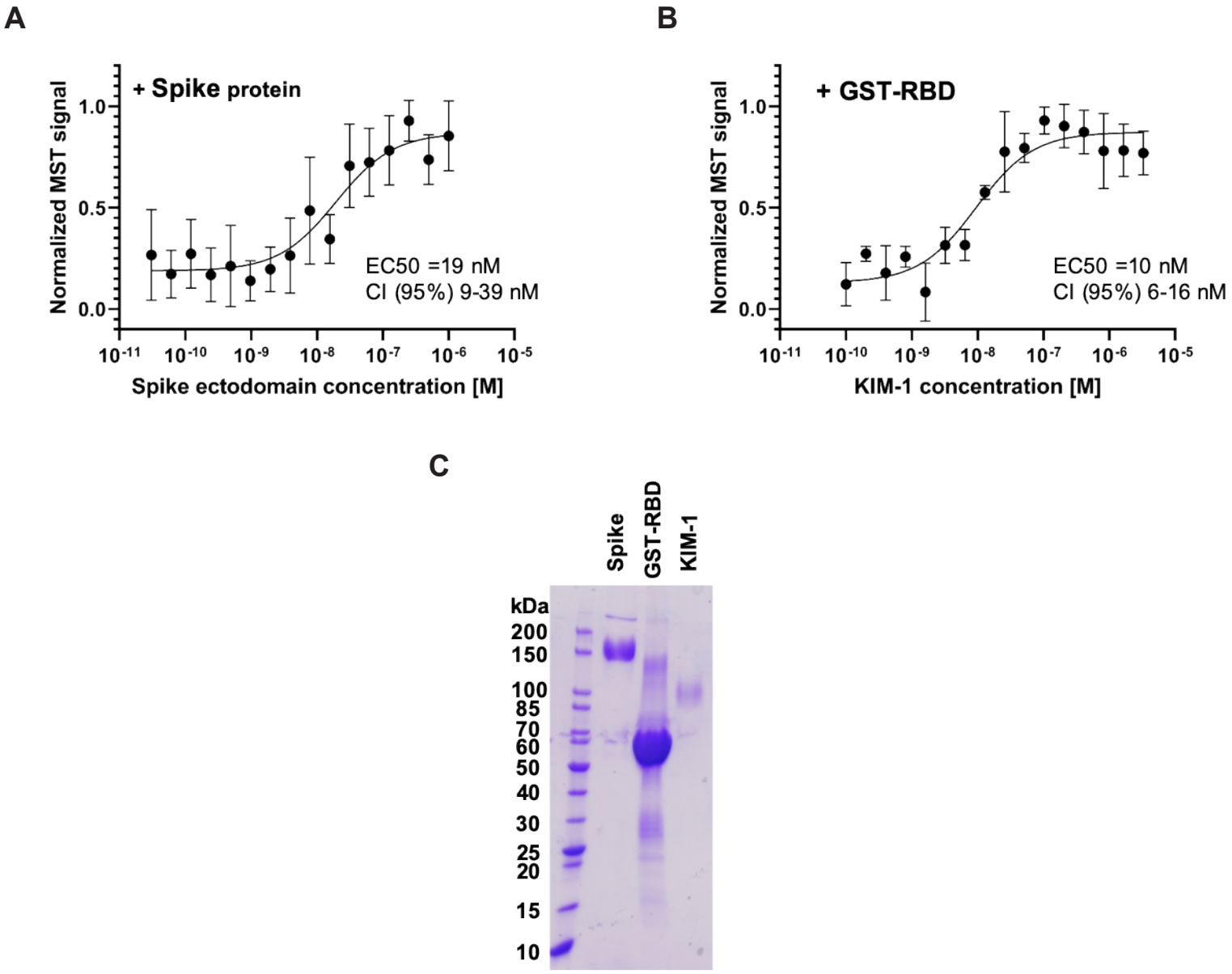
A
+ Spike protein
Normalized MST signal
1.0
0.5
0.0
EC50 =19 nM
CI (95%) 9-39 nM
10-11 10-10 10-9 10-8 10-7 10-6 10-5
Spike ectodomain concentration [M]
B
+ GST-RBD
Normalized MST signal
1.0
0.5
0.0
EC50 =10 nM
CI (95%) 6-16 nM
10-11 10-10 10-9 10-8 10-7 10-6 10-5
KIM-1 concentration [M]
C
Spike
GST-RBD
KIM-1
kDa
200
150
100
85
70
60
50
40
30
25
20
15
10

Figure 4